LAWRENCE
LIVERMORE
NATIONAL
LABORATORY

LLNL-JRNL-640598

O VIII H-alpha and Lyman-beta transitions as an XUV/EUV branching ratio tool

E. Trabert, P. Beiersdorfer, J. Clementson, A. Laska

July 8, 2013

The Astrophysical Journal Supplement Series

Disclaimer

O VIII H_α and Ly_β transitions as an XUV/EUV branching ratio tool

Elmar Träbert[1,2], Peter Beiersdorfer[1], Joel Clementson[1,3], and Alexander Laska[1,4]

Received _____; accepted _____

[1]Physics Division, Lawrence Livermore National Laboratory, Livermore, CA 94550-9234, USA

[2]also at Astronomisches Institut, Ruhr-Universität Bochum, 44780 Bochum, Germany

[3]now at MPI für Plasmaphysik, 17491 Greifswald, Germany

[4]also at Friedrich-Alexander-Universität Erlangen, 91054 Erlangen, Germany

ABSTRACT

A technique is described and evaluated to establish the relative response of spectroscopic detection systems in the XUV and the EUV. The procedure utilizes the 1s-3p and 2s-3p transitions in H-like ions and is illustrated in terms of the O VIII transitions located near λ16 (Ly_β) and λ102.4 (H_α). The procedure can provide an *in situ* reference for calibrating spectrometers in orbit. Radiative-collisional modeling is employed to disentangle the contributions to the O VIII H_α line. Laboratory observations test the validity of our model and indicate that significant corrections are necessary. The technique may also be used to check the spectrometer response in the laboratory when investigating the XUV excess that has been found for Capella.

Subject headings: atomic data — methods: laboratory — techniques: spectroscopic — ultraviolet: stars

1. INTRODUCTION

Observations of Capella (α Aurigae) have been made by diffraction grating spectrometers on board of various spacecrafts (*Extreme Ultraviolet Explorer EUVE, Far Ultraviolet Spectroscopic Explorer FUSE, Chandra, XMM − Newton*). The observed spectra have revealed discrepancies of relative line intensities measured in the soft-x-ray and extreme-ultraviolet (EUV) ranges versus various model predictions that were based on atomic data (Desai et al. 2005; Gu et al. 2006). Compared to some soft-x-ray (XUV) lines near 16 Å, some of the EUV lines near 100 Å appear more weakly in the observations of astrophysical objects than is expected from spectral modeling. The discrepancy may result from shortcomings of the atomic data or the spectrometer calibration, arise from peculiarities of spectral modeling, or it may reveal astrophysical phenomena at emission from the corona or with absorption by the interstellar medium. The latter effect, however, should amount to only a few percent in this case (Linsky et al. 1993; Piskunov et al. 1997) and has already been applied as a correction to the Capella data discussed (Desai et al. 2005; Gu et al. 2006). In the following we describe a technique for testing the spectrometer response in situ and present a laboratory measurement and an associated spectral calculation of the O VIII Ly$_\beta$ and H$_\alpha$ lines to illustrate the method. Future missions may combine sufficient spectral resolution and effective area so that the set of lines we describe can be seen in distant objects. Such observations can then effectively measure the interstellar absorption difference between the XUV and EUV ranges.

2. BRANCHING RATIO CALIBRATION SCHEME

Branching ratios of atomic transitions are a standard tool for establishing relative detection efficiencies in various spectral ranges (Huber & Sandeman 1980, 1986; Danzmann & Kock 1982; Denne & Hinnov 1984; Wiese et al. 1989). Many branching ratio data

result from comparison with light sources of well characterized spectral properties (such as synchrotron radiation), from atomic structure calculations, or from secondary observations. Elaborate light sources and procedures are typically used to calibrate instruments in the laboratory (Morgan et al. 1968; Hunter & Prinz 1977; Jacoby et al. 1981; Milchberg et al. 1986), but have limited use for in-orbit calibration. In contrast, the scheme we develop here is applicable to in-orbit calibrations. Our scheme is based on calculated values of a one-electron ion. These ions are considered well calculable by quantum mechanics. We make use of the decay branches of the 3p level of the hydrogen-like oxygen ion (spectrum O VIII), which are depicted schematically in Figure 1. The XUV branch is the Lyman-beta (Ly_β) line (transition 1s - 3p) at 16 Å which is composed of two lines, $3p_{1/2} \rightarrow 1s_{1/2}$ and $3p_{3/2} \rightarrow 1s_{1/2}$. The 2s - 3p transition ($3p_{1/2} \rightarrow 2s_{1/2}$ and $3p_{3/2} \rightarrow 2s_{1/2}$) is part of the Balmer-alpha (H_α) line at 102.4 Å. Both branches are $\Delta n > 0$ transitions. Quantum mechanical calculations indicate a branching ratio of 7.45 in favor of the XUV transition (Ly_β) that can be easily observed (Figure 2). Experimental problems, however, lie in the fact that the energy levels in low-Z H-like ions are almost degenerate, so that the two 2s-3p transitions of interest are part of the H_α transition array which also comprises two 2p-3s and three 2p-3d transitions, a total of 7 lines that cluster in two groups (Figure 3). As a consequence, the intensity ratio of the Ly_β to the H_α feature depends not only on a single branching ratio, but on all line formation mechanisms that can affect the 2p-3s and 2p-3d transitions relative to the 2s-3p transitions. The relative line intensities of the H_α line complex have already been discussed as a possible plasma diagnostic tool (Tallents 1984a,b, 1985). These contributions are not as accurately calculated as the branching ratio, and laboratory measurements are needed to test the models.

It is essential to find out what fraction of the observed full H_α line cluster signal actually represents the 2s-3p decay branch of interest under our low-density excitation conditions. In the following, the relative intensities of the XUV and EUV branches are

estimated by spectral modeling using the Flexible Atomic Code (FAC) (Gu 2008). We have used FAC to model the experimental plasma conditions found in our experiment (see section 3), which uses a quasi-monoenergetic electron beam with keV energies and an electron density near 10^{11} cm^{-3} to excite the O VIII spectrum.

The FAC model is based on relativistic distorted-wave calculations of electron-ion collisions some of which may lead to excitation and ionization, and comprises radiative transitions in a given ion, radiative recombination (RR) and dielectronic recombination (DR). The model calculations yield line-by-line emissivities (photons/ion/sec) which can be used to synthesize spectra. The model calculations were run for six electron beam energies ranging from one to twelve keV and for several electron beam densities (5×10^{10} to 5×10^{12} cm^{-3}). Our model reveals no notable dependence on the electron density in the range of densities we calculated. The reason is that there are essentially no metastable levels that may be affected by an increased collision rate as the electron density is raised.

Our calculations show that the effect of polarization as a result of the excitation by a unidirectional electron beam and observation at right angles to this beam amounts to a few percent at most, and that the contribution from radiative recombination (RR) processes is minute. There is the usual dependence on the electron beam energy in that overall the electron-impact collision cross sections decrease with increasing electron-ion interaction energies in the keV range. However, the collision-energy dependences of individual lines differ, and therefore the line intensity pattern is predicted to change within the range of electron beam energies from 1 to 12 keV as indicated in Figure 4.

The calculations show that the $3p \rightarrow 2s$ transitions are not the dominant components in the complete H_α feature. The strongest individual component (at lower electron beam energies) is the $3s_{1/2} \rightarrow 2p_{3/2}$ transition, which on its own accounts for about one quarter of the total intensity. The $3p_{3/2} \rightarrow 2s_{1/2}$ and $3p_{1/2} \rightarrow 2s_{1/2}$ transitions together are predicted

to make up more than one third of the H_α intensity. The 3d levels are predicted to be only weakly populated, in stark contrast to the high-density (actually, solid-state electron density) excitation studied in beam-foil spectroscopy (Müller et al. 1995). If, however, the H_α line cluster is partly resolved, both 2s-3p transitions of interest are falling into the short-wavelength line group, to which they contribute about half of the total signal and can be estimated with some confidence. This situation will be discussed in more detail in the measurement section below.

The branching ratio scheme for H-like O VIII allows a two-point calibration between 16 and 102 Å. The same scheme when applied to C VI allows calibration between 28.5 and 182 Å. Applying it to N VII and Ne X allows calibration between 21 and 134 Å and between 10 and 65 Å, respectively. Thus the H-like branching ratios can provide in-orbit checks on pre-flight calibrations performed in the laboratory, spanning a factor of three in wavelength in both the XUV and EUV ranges.

3. MEASUREMENT

Our measurement was performed at the Lawrence Livermore National Laboratory using the EBIT-I electron beam ion trap which is regularly employed for laboratory astrophysics measurements (Beiersdorfer 2003, 2008). In this device, a (quasi-) monoenergetic electron beam of adjustable energy serves to ionize and excite atoms under ultrahigh vacuum conditions (residual vacuum better than 10^{-11} mbar, electron density $n_e \approx 10^{11}$ cm^{-3}) approximating the dilute plasma conditions of stellar coronae. In order to produce an oxygen spectrum, carbon dioxide (CO_2) was injected ballistically into the vacuum vessel so that a gas plume of a central density below 10^{-8} mbar traversed the actual trap volume and the electron beam. By collisions with energetic electrons, the molecules were excited and broken up; positively charged fragments are trapped by the combination of drift tube

voltages, the electron beam space charge, and a strong magnetic field.

The measurements comprised XUV (14 - 20 Å) and EUV (92 - 107 Å) observations, made with two high-resolution flat-field spectrographs (Beiersdorfer et al. 2004) equipped with a variable line spacing grating of R=44.3 m and a groove density of about 2400 ℓ/mm, set at an angle of incidence of 87.5°. Cryocooled CCD cameras with 1300×1340 pixels (of 20 μm × 20 μm each) served as the detectors on both spectrographs. Sample spectra are shown in figures 2 and 3.

An electron beam of an energy of 3 keV produced spectra with prominent EUV and XUV lines of O VI, O VII, and O VIII for wavelength reference as well as for a calibration of the relative detection efficiency. The O VIII Ly$_\beta$ transition at λ16.006 can be observed without blending (see figure 2) and hence poses no evaluational problem. The fine structure splitting of the spectral line (two components) is far too small to be resolved by our observational means. In the EUV, a resolving power of $\lambda/\Delta\lambda \approx 3000$ of the instrument was reached which is in the same class as the LETGS transmission grating instrument onboard *Chandra*. High-resolution observations of the O VIII H$_\alpha$ line have been made before, under high- (Müller et al. 1995) and low-density conditions (our own high-resolution measurements of the O VIII H$_\alpha$ line emitted by trapped ions) (Träbert & Beiersdorfer 2013). An unidentified line appears at λ102.3 on the short-wavelength wing of the H$_\alpha$ line cluster (Figure 5), but it does not impede the analysis of the H$_\alpha$ line cluster components of interest. The seven components of the H$_\alpha$ line form two groups, with the four transitions to the $2p_{1/2}$ level making up the shorter-wavelength group and the three transitions to the $2p_{3/2}$ level the longer-wavelength one. The line broadening of each group (due to its composition) is evident in comparison to near-by other spectral lines, but the groups themselves are only partially resolved into their components.

For the analysis we assume that the calculations of the atomic structure of one-electron

systems are nearly perfect, and we adopt the energy level and wavelength values presented by Garcia & Mack (1965). The relative line intensities given by the FAC model calculations match the experimental line intensity pattern only moderately well (Figure 5 middle). However, the distribution of the components is such that even with only partly resolved lines it is possible to make sensible adjustments. The relative line intensities of the seven components of H_α can be described by six line ratios. Of these, two are branching ratios (same upper level) calculable by quantum mechanics, two relate to the fine structure (j-level) population of a given term which can be approximated by the statistical weights (see below), and two relate the ℓ levels (P and D terms) to the s level population. The principal observational parameters are the relative intensities of the two major line groups of the H_α line and the relative intensities of the two peaks of the long-wavelength line group. The latter line ratio is dominated by the single $3d_{5/2}$ level decay and the stronger branch of the $3s_{1/2}$ level decay. The weaker branch of the $3s_{1/2}$ level decay, to the $2p_{1/2}$ level, is quantum mechanically known to be half as strong. In the short-wavelength line group, the upper levels of the 2s-$3p_{1/2,3/2}$ level decays may be assumed to reflect the statistical weights (Orstein & Burger 1924) and thus show a line ratio of 1 : 2. A similar argument is assumed for the relative populations of the $3d_{3/2,5/2}$ levels. (The FAC model produces level populations close to these ratios for electron beam energies of 2 keV and higher, but clearly differs at 1 keV. It should be noted that Tallents (1984a,b) assumes statistical level populations only at much higher densities.) Thus only two parameters, one for the 3p levels and one for the 3d levels, are considered free in relation to the 3s level population. Taking the FAC results as a starting point and modifying the relative line intensities of the contributions from the 3p and 3d level decays (compared to 3s) it is possible to obtain a reasonably good match of the model with the relative intensities of the two line groups and of the recognizable detail features (see the bottom part of Figure 5). Our best fit implies an increase of the assumed 3d emissivities by 70% and a decrease of the 3p emissivities by

25% (relative to the 3s $\rightarrow$ 2p decay). This result in turn yields information on the actual level populations and on the modeling process.

In our spectra the signal (emissivity) is proportional to the transition rate and the upper level population. We use this relation to obtain the relative level populations from the observed signal, taking the transition rates for H atoms given by Wiese et al. (1966) and scaling those with the fourth power of the nuclear charge Z. These values are practically reproduced by the FAC calculations. Of the 3p level decays we only see a 13% fraction in the H_α line profile. The remaining intensity is in the Ly_β line. However, we do not yet know the XUV/EUV detection efficiency ratio. Therefore we add the level population fraction that corresponds to the XUV branch of the 3p levels not from the XUV observation, but in the quantum mechanically prescribed ratio to the observed EUV decay branch. Our experimental results for the n=3 level populations are compared to the FAC model predictions in Figure 6. The 3s level is populated the most, but because of the longer level lifetime (39 ps) (lower decay rate) the signal of its decay branches is commensurate with the signals of the 3p (lifetime 1.29 ps) and 3d level (lifetime 3.8 ps) decays. The associated error bars reflect the ambiguity in the trial-and-error matching of the predicted H_α components to the complete line profile.

4. COMPARISON BETWEEN THEORY AND MEASUREMENT

Figure 6 shows that the predicted relative populations of the 3s and 3p fine structure levels vary significantly at electron beam energies of a few keV. The predicted relative level population of the 3p levels amounts to about 0.45 of the total at 1 keV and to about 0.6 at 10 keV and higher. Figure 6 shows that the experimental level population pattern and the collisional-radiative simulation (by FAC) do agree only moderately well. Evidently, the experimental level population pattern at 3 keV electron beam energy is

better approximated by the values calculated for half that energy. On one hand this match shows a reasonable agreement between modeling and experiment, on the other there appear significant shortcomings of the simulation.

For our branching ratio technique, we need to know the fraction of the H_α line signal that originates from the 2s-3p transitions. Our collisional-radiative model predicts that a fraction of 0.36 of the whole H_α line intensity originates from the 2s-3p transitions at an electron beam energy of 3 keV (a fraction of 0.41 is indicated by the FAC calculations for an electron beam energy of 6 keV). After adjusting the level populations to match our observed spectrum, the revised model indicates that a fraction of only 0.25±0.01 of the observed O VIII H_α signal at λ102.4 relates to the 2s-3p transition and can be used in combination with the 7.45 : 1 branching ratio of the two decay channels of the 3p levels to establish the XUV/EUV detection efficiency ratio. (If one evaluates not the full H_α line cluster, but only the short-wavelength line group, the FAC prediction of the 2s-3p transitions amounts to a fraction of 0.63, which is changed in our experiment to 0.506±0.02.) That is a significant change from *ab initio* modeling by one third when referring to the complete H_α line cluster (one fifth when referring only to the short-wavelength component). The error bar reflects the uncertainty of the ajustment process, in which the derived fraction turns out to be not very sensitive to the details of the line intensity pattern assumed.

For all practical means, the 3p → 1s / 3p → 2s branching ratio is exactly determined by quantum mechanics. The fraction of the H_α line signal that originates from the 2s-3p component can be determined reliably from experiment, if the spectral resolution is at least as high as in our experiment. The uncertainty of the application of the branching ratio to the determination of the XUV vs. EUV response of the detection equipment at the two wavelengths, λ16 and λ102.4, respectively, is then directly linked to the signal statistics, but independent of the excitation process.

5. DISCUSSION

We have observed a partially resolved O VIII H_α line profile and analyzed the contributions with a view to exploiting the 1s-3p / 2s-3p branching ratio for a calibration of detection systems that connects the XUV and the EUV ranges. Depending on the actual spectral resolution, the interpretation of the experiment requires collisional-radiative modeling. Our spectral data are well enough resolved to recognize and largely overcome shortcomings of the modeling and to validate the proposed XUV/EUV calibration procedure. Although we take guidance from a collisional-radiative model, our evaluation actually does without, but makes a few minor assumptions about fine structure level populations that are corroborated by the model predictions.

With even higher spectral resolution than our equipment afforded, it should be possible to study the level populations of all individual fine structure levels and thus to perfect the investigations of the modeling process. If one does not resolve the components of the H_α line, the fraction made up by the 2s-3p decays can be obtained only from collisional-radiative modeling. In our example, the model predicts a fraction 50% higher than warranted by the experimental evidence.

However, beyond its present use, collisional-radiative modeling can help to expand the applicability of the technique in other ways. Figure 3 shows a line series in O VI. Within the confidence limits of predictions by a collisional-radiative model of the n-dependence of the emissivities, this line series provides a ruler to determine the trend of the detection efficiency over the wavelength range λ92 to λ105. Correspondingly (see Figure 2) there are the O VIII and O VII resonance line series in the XUV, which may yield a calibration curve for the XUV range from about λ14 to λ22 (as presented by Beiersdorfer et al. (2004)), and correspondingly for H-like ions of other elements.

This work was performed under the auspices of the U.S. Department of Energy by Lawrence Livermore National Laboratory under Contract DE-AC52-07NA27344 and was supported by the Astrophysics Research and Analysis Program of the National Aeronautics and Space Administration. E.T. acknowledges support from the German Research Association (DFG) (grants Tr171/18 and Tr171/19).

REFERENCES

Beiersdorfer, P. 2003, ARA&A, 41, 343

Beiersdorfer, P. 2008, Can. J. Phys., 86, 1

Beiersdorfer, P., Magee, E. W., Träbert, E., Chen, H., Lepson, J. K., Gu, M.-F., & Schmidt, M. 2004, Rev. Sci. Instrum., 75, 3723

Danzmann, K., & Kock, M. 1982, J. Opt. Soc. Am., 72, 1556

Denne, B., & Hinnov, E. 1984, J. Opt. Soc. Am. B, 1, 699

Desai, P., Brickhouse, N., Drake, J. J., Dupree, A. K., Edgar, R. J., Hoogerwerf, R., Kashyap, V., Wargelin, B. J., Smith, R. K., Huenemoerder, D. P., & Liedahl, D. A. 2005, ApJ, 625, L59

Garcia, J. D., & Mack, J. E. 1965, J. Opt. Soc. Am., 55, 654

Gu, M. F., Gupta, R., Peterson, J. R., Sako, M., & Kahn, S. M. 2006, ApJ, 649, 979

Gu, M. F. 2008, Can. J. Phys., 86, 675

Huber, M. C. E., & Sandeman, R. J. 1980, Phys. Scr., 22, 373

Huber, M. C. E., & Sandeman, R. J. 1986, Rep. Prog. Phys., 49, 397

Hunter, W. R., & Prinz, D. K. 1977, Appl. Opt., 16, 3171

Jacoby, D., Pert, G. J., Shorrock, L. D., & Tallents, G. J. 1981, J. Phys. E, 14, 1061

Kelly, R. L. 1987, J. Phys. Chem. Ref. Data, 16, Suppl. No. 1

Linsky J. L., Brown, A., Gayley, K., Diplas, A., Savage, B. D., Ayres, T. R., Landsman, W., Shore, S. N., Heap, S. R. 1993, ApJ, 402, 694L

Morgan, F. J., Gabriel, A. H., & Barton, M. J. 1968, J. Sci. Instrum., 1, 998

Milchberg, H., Skinner, C. H., Suckewer, S., & Voorhees, D. 1986, Rev. Sci. Instrum., 57, 3057

Müller, H. R., Heckmann, P. H., & Träbert, E. 1982, Z. Phys. A, 308, 283

Ornstein, L. S., & Burger, H. C. 1924, Z. Phys, 24, 41

Piskunov, N., Wood, B. E., Linsky, J. L., Dempsey, R. C., & Ayres, T. R. 1997, ApJ, 474, 315p

Tallents, G. J. 1984, Phys. Rev. A, 29, 3461

Tallents, G. J. 1984, J. Phys. B, 17, 3677

Tallents, G. J. 1985, J. Phys. B, 18, 3299

Träbert, E. & Beiersdorfer, P. 2013, Phys. Scr. T, 15x, xxx (in print)

Wiese, W. L., Smith, M. W., & Glennon, B. M., 1966, Atomic Transition Probabilities. Volume I Hydrogen Through Neon. NSRDS-NBS4, Washington, DC

Wiese, W. L., Brault, J. W., Danzmann, K., Helbig, V., & Kock, M. 1989, Phys. Rev. A, 39, 2461

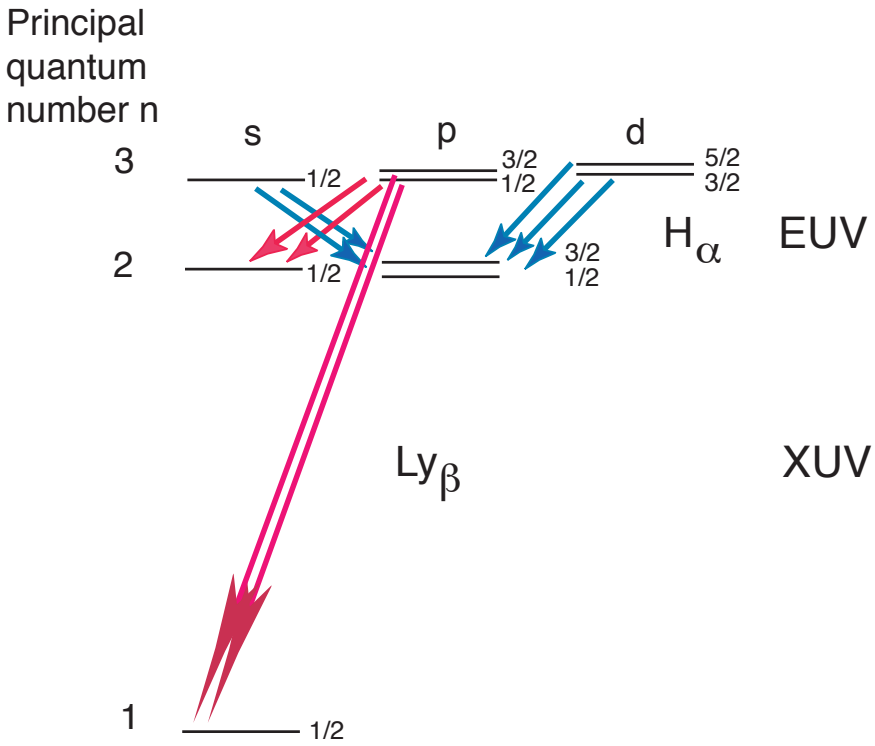

Fig. 1.— Level and decay scheme for n=3 levels in an H-like ion such as O VIII.

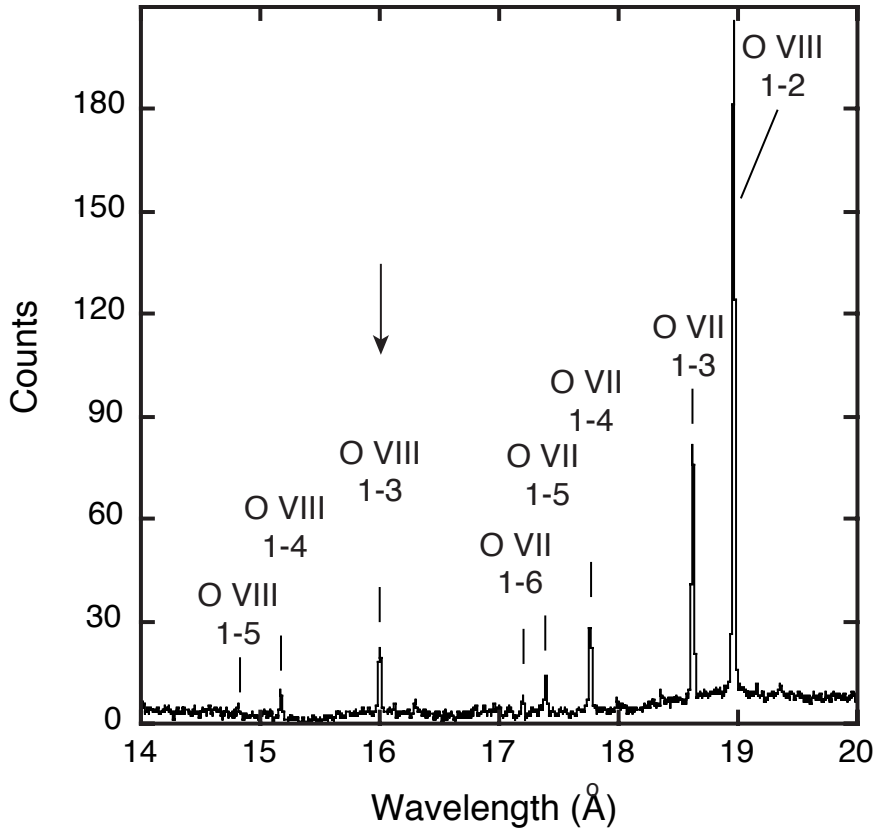

Fig. 2.— Spectrum of oxygen in the range 14 to 20 Å recorded with a high-resolution grating spectrograph at the EBIT-I electron beam ion trap. The O VII $1s^2$ - $1snp$ and O VIII 1s - np line series are marked. The arrow points to the Ly_β line. The electron beam energy was 3 keV.

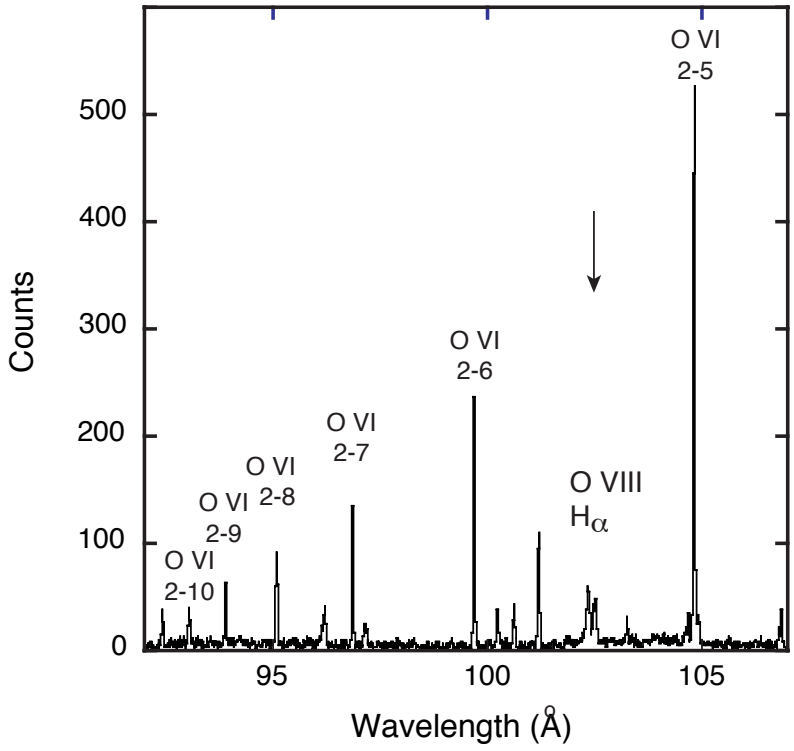

Fig. 3.— Spectrum of oxygen in the range 92 to 107 Å recorded with a high-resolution grating spectrograph at the EBIT-I electron beam ion trap. The arrow points to the double feature of the H_α line. The electron beam energy was 3 keV.

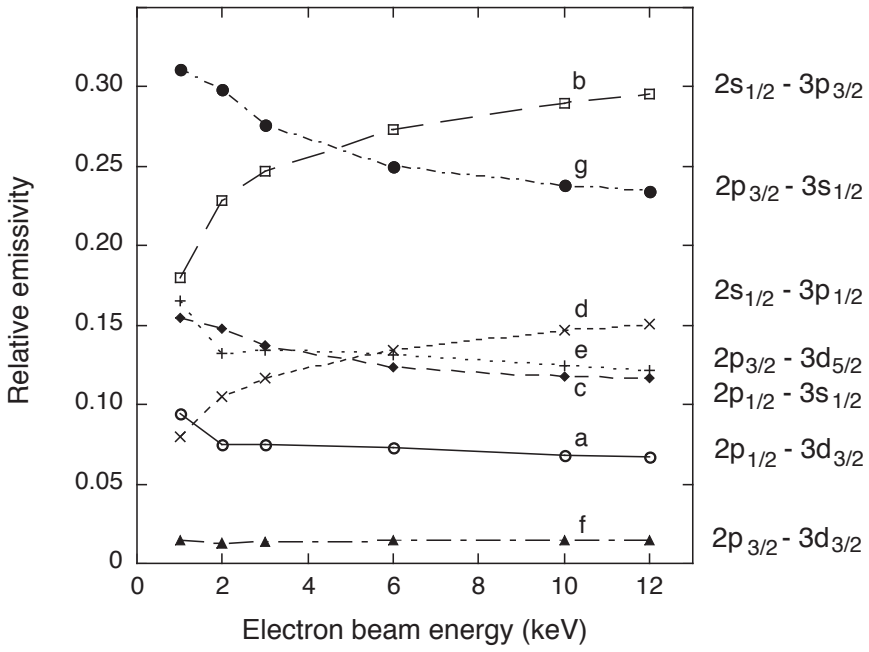

Fig. 4.— Emissivity (photons/s/ion) predictions by collisional-radiative modeling using FAC for the seven components of the O VIII H_α line as a function of electron beam energy. The raw data have been corrected for polarization effects due to the excitation by a unidirectional electron beam as well as for radiative recombination, and then normalized to the sum of emissivities predicted for the H_α line array. The seven multiplet components are labeled alphabetically in the sequence of increasing wavelengths.

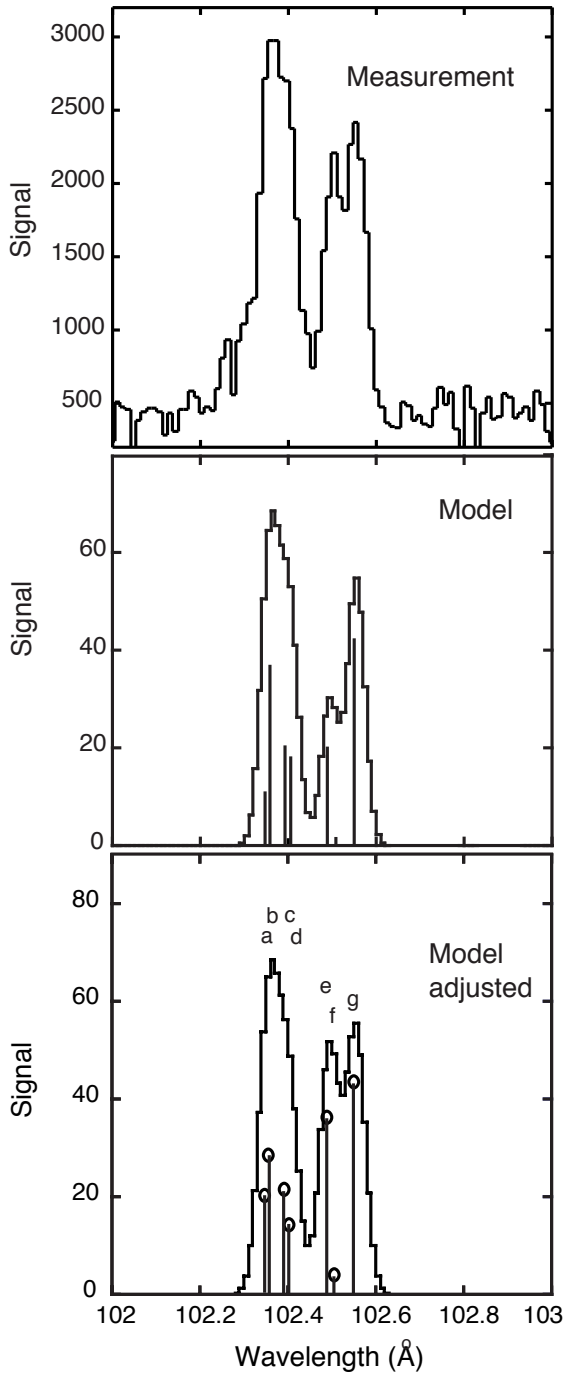

Fig. 5.— Top: O VIII H_α line profile measured at an electron beam energy of 3 keV. Middle: Relative line intensities of the seven components of the O VIII λ102.4 line predicted by FAC for excitation at 3 keV, plus a synthetic line profile based on these adjusted components. Bottom: The same after adjustment of the emissivities to match the measured line profile (see text). The seven multiplet components are (in the sequence of increasing wavelengths) a) $2p_{1/2}$-$3d_{3/2}$, b) $2s_{1/2}$-$3p_{3/2}$, c) $2p_{1/2}$-$3s_{1/2}$, d) $2s_{1/2}$-$3p_{1/2}$, e) $2p_{3/2}$-$3d_{5/2}$, f) $2p_{3/2}$-$3d_{3/2}$, and g) $2p_{3/2}$-$3s_{1/2}$.

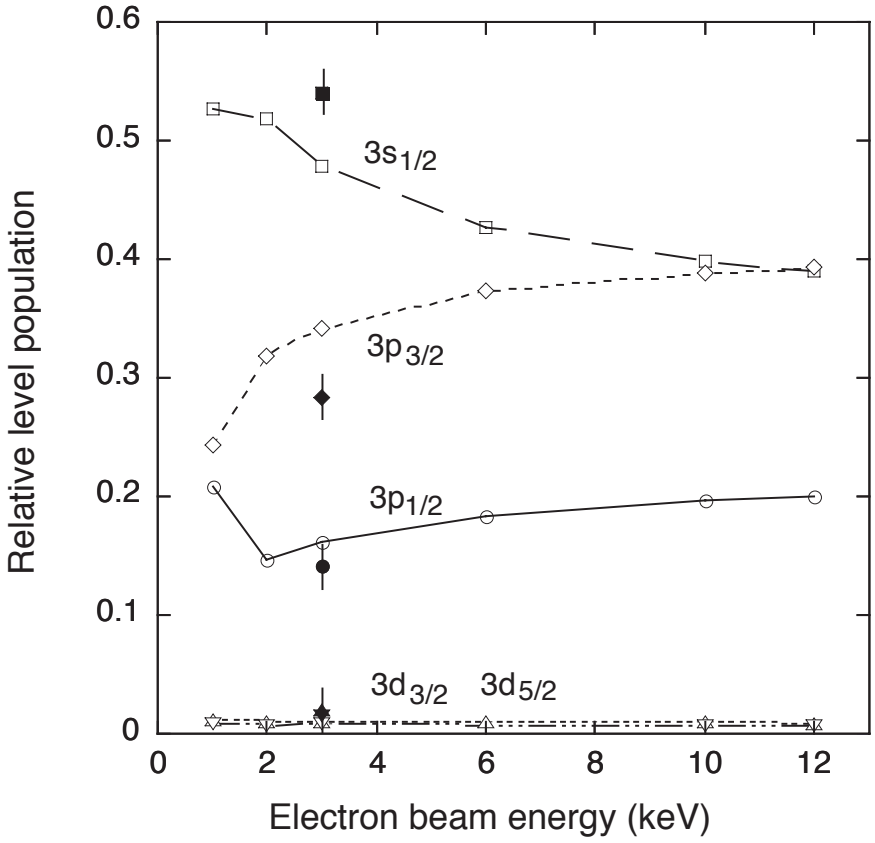

Fig. 6.— $n = 3$ level populations of O VIII as a function of electron beam energy and normalized to the sum. Open symbols: Predictions by collisional-radiative modeling using FAC, full symbols: measurement at an electron beam energy of 3 keV. The error bars are estimates.